

Emission and excitation characteristics and internal quantum efficiencies of vacuum-ultraviolet excited Pr³⁺-doped fluoride compounds

Stefan Kück,^{1,*} Irena Sokólska,^{2,3} Markus Henke,³ Thomas Scheffler,³ and Eugen Osiaç^{3,4}

¹Physikalisch-Technische Bundesanstalt, Abteilung Optik, Bundesallee 100, 38116 Braunschweig, Germany

²Institute of Low Temperature and Structure Research, Polish Academy of Sciences 50-950 Wrocław, Poland

³Universität Hamburg, Institut für Laser-Physik, Luruper Chaussee 149, 22761 Hamburg, Germany

⁴Institute of Atomic Physics, P.O. Box. MG-6, 76900 Bucharest, Romania

(Received 14 September 2004; published 20 April 2005)

We report on the spectroscopic investigation of Pr³⁺-doped binary, ternary, and quaternary fluoride compounds exhibiting photon cascade emission. Under vacuum-ultraviolet synchrotron excitation at wavelengths below 200 nm in the 4f5d bands of the Pr³⁺ ion the emission spectra show intraconfigurational 4f-4f transitions originating from the ¹S₀ and ³P₀ multiplets. In the ternary and quaternary compounds investigated, i.e., Ca-, Sr-, Ba-, and Rb-fluorides, broadband emission due to transitions from the 4f5d level of Pr³⁺ are also observed. The different types of emission transitions observed in the compounds investigated were analyzed in detail. The internal quantum efficiency for the visible spectral range (390 nm–750 nm), η_{vis} , is determined with the help of the Judd-Ofelt theory and the branching ratios of the ¹S₀ emission transitions. The dependence of this quantum efficiency η_{vis} from the ionic radius of the second cation ($R_{2\text{nd}}$), the effective ligand distance, and the coordination number is investigated.

DOI: 10.1103/PhysRevB.71.165112

PACS number(s): 78.55.-m, 42.70.-a, 71.55.-i, 78.20.-e

I. INTRODUCTION

Luminescent materials with a quantum efficiency higher than unity might play a significant role for lighting applications, especially in discharge lamps. Environmental reasons may force the replacement of mercury gas by xenon gas. The latter emits at wavelengths around 172 nm, thus at shorter wavelengths compared to the Hg discharge, where the mean emission wavelength is around 243 nm. Therefore, the phosphors to be used in the Xe-discharge lamp need to have a photon conversion efficiency of 140% of that for the commonly used phosphors. Since the latter have photon conversion efficiencies of approximately 90%, the Xe-discharge phosphors need to have an average photon conversion efficiency of approximately 125%. Thus, the challenge of this ongoing work is the development of efficient luminescent materials which compensate for the additional energy required when using the Xe discharge. Suitable materials are so called “quantum cutters” or “photon cascade emitters,” which generate more than one visible photon after absorbing a vacuum-ultraviolet (VUV) or ultraviolet (UV) photon.

Besides the recently found quantum cutters, such as Eu³⁺:LiGdF₄ and Er³⁺, Tb³⁺:LiGdF₄,^{1,2} Pr³⁺-doped materials with their well separated energy levels are promising candidates for this mechanism. The photon cascade emission was observed in YF₃ by Sommerdijk *et al.*^{3,4} and Piper *et al.*⁵ The energy-level scheme of Pr³⁺:YF₃ is shown in Fig. 1. After an efficient optical absorption into the 4f5d bands at a wavelength below 200 nm, the energy is nonradiatively transferred to the ¹S₀ level of the 4f manifold, which is the starting level of the two-step emission process. The first step of this cascade is the ¹S₀→¹I₆ transition in the blue spectral range around 400 nm. This transition has a branching ratio of 60–80 %, depending on the host material. It is followed—after thermal relaxation into the ³P_{0,1} levels—by the second

step, i.e., the ³P_{0,1}→³F_J, ³H_J transitions. These transitions are accompanied almost completely by visible emission (see also Fig. 1). The condition for the cascade emission to occur is that the 4f5d level is located energetically above the ¹S₀ level, which is located approximately at 46 500 cm⁻¹.

The visible emission from the ³P₀ level is very suitable with respect to the spectral sensitivity of the human eye, however, the blue emission from the first step occurs at a too short wavelength. Until now an efficient conversion into the visible spectral range was not successful without losing the overall quantum efficiency > 1.

In this paper we focused on Pr-doped yttrium, lutetium, and lanthanum fluoride compounds. We investigated a series of materials with different coordination numbers, different

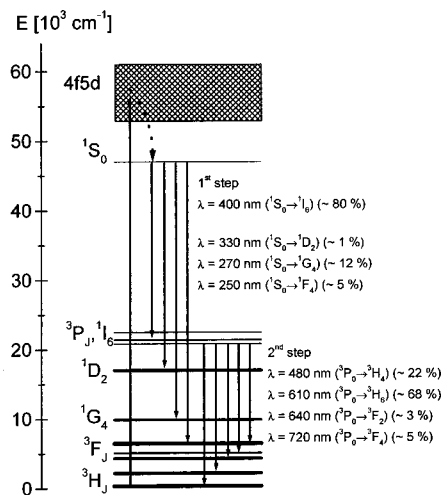


FIG. 1. Energy-level scheme of Pr³⁺:YF₃. The transition branching ratios for the main transitions of the cascade are also given (Refs. 5 and 32).

TABLE I. Materials investigated, Pr^{3+} concentration in the melt, results of the investigation of the phase purity, and type of emission. *PCE*: exhibits cascade emission, *5d*: exhibits *5d* emission; *TC*: thermally activated *5d* emission; *OC*: at least two optical centers observed. *: in the melt, real concentration much lower.

No.	Compound	Pr^{3+} concentration (at%)	Phase	Type
1	YF_3	0.13	OK	PCE (Refs. 3–5)
2	NaYF_4	0.08	OK	PCE (Refs. 3,4)
3	LaF_3	0.2	OK	PCE (Ref. 7)
4	NaLaF_4	0.08	OK	PCE (Ref. 5)
5	LuF_3	0.2	OK	PCE (Ref. 9)
6	KMgF_3	0.15*	single crystal	PCE (Ref. 6), OC (Ref. 15)
7	BaMgF_4	0.2	OK	PCE (Ref. 9)
8	PrF_3		OK	PCE (Ref. 10)
9	$\text{Ca}_{0.9}\text{Y}_{0.1}\text{F}_{2.1}$	0.02	OK	PCE, <i>5d</i> , OC
10	$\text{Na}_{0.9}\text{Ca}_{0.9}\text{Y}_{1.1}\text{F}_6$	0.05	OK	PCE, <i>5d</i> , OC
11	$\text{Ca}_{0.65}\text{La}_{0.35}\text{F}_{2.35}$	0.05	OK	PCE, <i>5d</i> , OC
12	$\text{Na}_{0.8}\text{Ca}_{0.8}\text{La}_{1.2}\text{F}_6$	0.05	not analyzed	PCE, <i>5d</i> , OC
13	$\text{Ca}_{2.028}\text{Lu}_{0.972}\text{F}_7$	0.01	OK	PCE, <i>5d</i> , OC
14	SrYF_5	0.07	not identified	PCE, <i>5d</i> , TC, OC
15	$\text{Sr}_{0.69}\text{La}_{0.31}\text{F}_{2.31}$	0.05	not identified	PCE, <i>5d</i> , OC
16	$\text{Ba}_4\text{Y}_3\text{F}_{17}$	0.06	OK	PCE, <i>5d</i> , TC, OC
17	$\text{Ba}_{0.5}\text{La}_{0.5}\text{F}_{2.5}$	0.05	OK	PCE, <i>5d</i> , TC, OC
18	Rb_3YF_6	0.05	not analyzed	PCE, <i>5d</i> , TC, OC
19	$\text{RbLu}_3\text{F}_{10}$	0.05	crystalline not analyzed	PCE, <i>5d</i> , OC

ionic radii of the second cation, and different ionic distances in order to analyze their effects on the quantum efficiency.

II. MATERIALS SELECTION AND PREPARATION

From literature studies, e.g., Refs. 6–13, and also from preliminary investigations in our research group it was assumed that there are several requirements for the host lattice of the Pr^{3+} ion in order to provide a cascade emission. From the physical point of view, a high coordination number of the Pr^{3+} ion leads to a small crystal-field splitting of the *4f5d* states. This can be explained by the fact that for a higher number of nearest neighbors the spherical-symmetric part ϵ_0 of the crystal-field perturbation increases, whereas the non-spherical-symmetric part, expressed by the energetic splitting caused by the crystal field Δ , decreases,

$$\epsilon_0(6) = \frac{3}{4}\epsilon_0(8) = \frac{1}{2}\epsilon_0(12),$$

$$\Delta(6) = -\frac{9}{8}\Delta(8) = -2\Delta(12),$$

where the number in brackets represents the coordination number (6 for an octahedron, 8 for a cube, and 12 for a cube-octahedron). As a result, a higher coordination number leads to a more elevated *4f5d* configuration and a reduced splitting of the energy levels. This of course favors a situation in which the *4f5d* levels are energetically higher than the 1S_0 level of the *4f²* configuration. A large radius of the substituted lattice site reduces the crystalline field and thus also favors cascade emission. Also it was found that a small

radius ($< \sim 1.4 \text{ \AA}$) of a second cation present in the compound supports cascade emission. This observation can be explained by the nephelauxetic effect. From the phenomenological point of view, possible cascade emitters can be found by looking at the energy-level schemes of Ce^{3+} . Dorenbos^{12,13} showed for a large number of materials that the energetic positions of the lowest *4f5d* band of all the rare-earth ions within a specific host material are correlated to each other. For the Pr^{3+} ion the following relation between the lowest states of the *4f5d* levels of Ce^{3+} and Pr^{3+} , $E(\text{Ce}^{3+}, 5d)$ and $E(\text{Pr}^{3+}, 4f5d)$, holds:

$$E(\text{Pr}^{3+}, 4f5d) = E(\text{Ce}^{3+}, 5d) + 12\,240 \text{ cm}^{-1} \pm 750 \text{ cm}^{-1}.$$

Thus we chose a variety of materials, which fulfilled the above-described conditions or looked promising, according to the phenomenological results obtained by Dorenbos. These materials were the known pure cascade emitters YF_3 , NaYF_4 , LaF_3 , NaLaF_4 , LuF_3 , KMgF_3 , BaMgF_4 , PrF_3 , the Ca-compounds $\text{Ca}_{0.9}\text{Y}_{0.1}\text{F}_{2.1}$, $\text{Na}_{0.9}\text{Ca}_{0.9}\text{Y}_{1.1}\text{F}_6$, $\text{Ca}_{0.65}\text{La}_{0.35}\text{F}_{2.35}$, $\text{Na}_{0.8}\text{Ca}_{0.8}\text{La}_{1.2}\text{F}_6$, $\text{Ca}_{2.028}\text{Lu}_{0.972}\text{F}_7$, and the Sr-compounds SrYF_5 , and $\text{Sr}_{0.69}\text{La}_{0.31}\text{F}_{2.31}$. Furthermore, we also investigated the Ba-compounds $\text{Ba}_4\text{Y}_3\text{F}_{17}$ and $\text{Ba}_{0.5}\text{La}_{0.5}\text{F}_{2.5}$ and the Rb-compounds, Rb_3YF_6 and $\text{RbLu}_3\text{F}_{10}$, which do not fulfill all the conditions stated above.

Most of the materials were prepared by stoichiometrically mixing the starting materials. The Pr concentrations in the melt are given in Table I. After heating them above the melting temperature and slowly cooling them down to room tem-

perature, polycrystalline or single crystalline samples were obtained. The purity of the phases of most of the compounds was inspected by the University of Cologne using the powder diffraction method (see also Table I). In some cases the structure analysis revealed different compounds than intended. In these cases the starting materials were mixed according to the results of the structure analysis, and they were newly prepared. In the case of KMgF_3 a single crystal was grown by the Czochralski method. The results of the structure analysis are summarized in Table I.

III. EXPERIMENTAL SECTION

The spectroscopic investigations were carried out at the SUPERLUMI station of HASYLAB (Hamburger Synchrotron Laboratorium) at DESY (Deutsches Elektronen-Synchrotron) in Hamburg. For details of the experimental setup see Refs. 10 and 14. The experiments were performed at room temperature (RT) and at 10 K. The spectral range of the excitation measurements was 100 nm–350 nm (12.4 eV–3.5 eV) with a resolution of 0.3 nm. The excitation spectra were corrected for the photon flux of the excitation beam by using the excitation spectrum of sodium salicylate ($\text{C}_7\text{H}_5\text{NaO}_3$) as the standard. The emission spectra were measured with two setups. In the 200 nm–800 nm spectral range a 0.3 m monochromator (Acton Research Corp., SpectraPro-308) and a CCD camera (Princeton Instruments Inc.) were used. Additionally, in the 200 nm–300 nm range the same 0.3 m monochromator and a photomultiplier (Hamamatsu R6358) were used. In the setup with the photomultiplier a time-dependent measurement is possible by using different time windows for the detector responses. The time-integrated, short-time window and long-time window measurements covered time intervals of 0–192 ns, 0–40 ns, and 100–192 ns, respectively. Thus the short-time and long-time emission spectra allow discrimination between $5d$ transitions (decay times typically <20 ns) and $4f$ transitions (decay times typically $\sim\mu\text{s}$ for 1S_0 decays). The resolutions of the emission spectra are approximately 0.5 nm, if not otherwise stated in the figure captions.

For both setups the correction curves in the spectral range between 200 nm and 450 nm were not available at the time of the experiments. Therefore, a different correction procedure was carried out, as it was performed in (Ref. 6). The photon fluxes of the Pr^{3+} emission bands in $\text{Pr}^{3+}:\text{YF}_3$ originating from the 1S_0 and 3P_0 level were measured by Piper *et al.* and are given in (Ref. 5). Thus, by comparing the branching ratios β measured in our experiments for $\text{Pr}^{3+}:\text{YF}_3$ with those results, the correction factors C for the specific wavelength regions were determined [$\beta(\text{YF}_3) = C\beta_{\text{exp}}(\text{YF}_3)$]. These correction factors were then used for the determination of the 1S_0 branching ratios of the material investigated [i.e., $\beta(X) = C\beta_{\text{exp}}(X)$] and the theoretical quantum efficiency.

The kinetics of the emission decays were measured by a standard single-photon counting method. The determination of the decay of the emission was limited by the period of 192 ns between the synchrotron radiation bunches. Therefore the decay times given in this paper have to be considered as estimates.

IV. SPECTROSCOPIC RESULTS—EMISSION SPECTRA

All investigated materials exhibited photon cascade emission. However, except for YF_3 , NaYF_4 , LaF_3 , NaLaF_4 , LuF_3 , and BaMgF_4 , all compounds also showed a broadband emission at room temperature. In order to find out whether this broadband emission was caused by the thermal coupling between the 1S_0 level and the $4f5d$ levels, emission spectra were also taken at a temperature of 10 K, and the emission decay curves were measured. In the case of a wavelength-independent decay characteristic, it was assumed that only one emitting center existed in the compound. In case of a wavelength-dependent decay, at least two centers were present in the compound. In the following the different compounds investigated will be discussed.

A. Pure cascade emitters

Among the materials investigated, the compounds YF_3 , NaYF_4 , LaF_3 , NaLaF_4 , LuF_3 , and BaMgF_4 exhibited pure photon cascade emissions with no influence from other emissions such as $5d$, host, or impurity emissions (see Fig. 2). For PrF_3 also a broadband emission between 260 nm and 320 nm was observed, most probably due to a host transition.¹⁰ Recently, also for KMgF_3 , a second emission center was observed exhibiting a broadband emission.¹⁵ In the emission spectra [Fig. 2(a)], bands at about 250 nm, 270 nm, 335 nm, and 400 nm were observed, which are characteristic for the transitions from the 1S_0 to the 3F_4 , 1G_4 , 1D_2 , and 1I_6 multiplets, respectively. The branching ratios for these transitions were on the order of ~ 5 –10%, ~ 10 –25%, ~ 2 –15%, and ~ 60 –80%, respectively. In all materials, the $^1S_0 \rightarrow ^1I_6$ transition around 400 nm was clearly the strongest. The emission bands around 480 nm, 530 nm, 610 nm, 640 nm, 690 nm, and 710 nm belonged to the transitions between the 3P_0 level (and thermally coupled 3P_1 level) to the 3H_4 , 3H_5 , 3H_6 , 3F_2 , 3F_3 , and 3F_4 levels, respectively. In the emission spectra taken within the spectral range of 200–300 nm additional emission lines were observed due to the transitions from 1S_0 to the 3H_4 , 3H_5 , 3H_6 , and 3F_2 levels [see Fig. 2(b)], located at about 215 nm, 225 nm, 236 nm, and 242 nm, respectively. The transition to the 3F_3 level was expected to be at 249 nm and was observed in some materials as a small shoulder in the $^1S_0 \rightarrow ^3F_4$ emission line. In general, all these transitions were weak, and the sum of their transition branching ratios is on the order of a few percent.

The Pr^{3+} ion substituted for the trivalent rare-earth-ion site in the lattices investigated. A substitution for the Na^+ or Mg^{2+} site was not expected from the consideration of the ionic radii [see Table II (data taken from Ref. 16)], and also was not observed. Together with the known PCE compounds LaZrF_7 , $\alpha\text{-LaZr}_3\text{F}_{15}$,¹⁷ and BaSiF_6 (Ref. 18) they all fulfilled the characteristics stated in Sec. II, with only one possible site for the Pr^{3+} ion, a small radius of the second cation ($<1.4 \text{ \AA}$) (note that in case of just one cation its radius was taken into account), and a high coordination number (≥ 8) (see Table III).

B. Ca compounds

The overview emission spectra of the Ca compounds investigated, i.e., $\text{Ca}_{0.9}\text{Y}_{0.1}\text{F}_{2.1}$, $\text{Na}_{0.9}\text{Ca}_{0.9}\text{Y}_{1.1}\text{F}_6$,

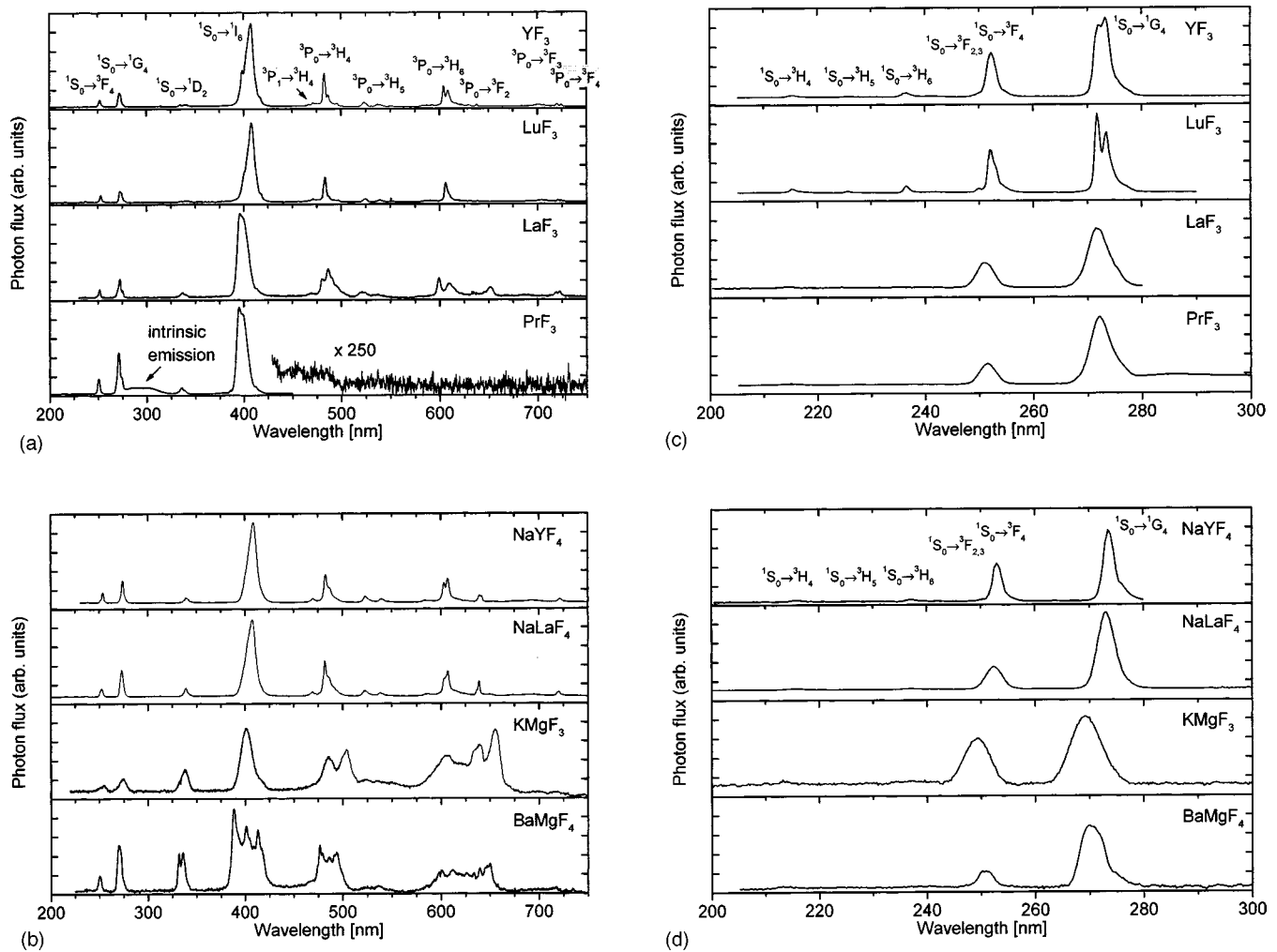


FIG. 2. Room-temperature emission spectra (uncorrected) under excitation at approximately 190 nm (KMgF₃: 172 nm) of the pure cascade emitters YF₃, NaYF₄, LaF₃, NaLaF₄, LuF₃, KMgF₃, BaMgF₄, and PrF₃. (a) 200 nm–750 nm (CCD camera). (b) 200 nm–300 nm (photomultiplier or CCD camera, resolution approximately 0.3 nm).

Ca_{0.65}La_{0.35}F_{2.35}, Na_{0.8}Ca_{0.8}La_{1.2}F₆, and Ca_{2.028}Lu_{0.972}F₇, are shown in Fig. 3(a). The transitions from the ¹S₀ level as well as those from the ³P₀ level are clearly observed, indicating photon cascade emission. Looking in detail into the short-wavelength spectra [see Fig. 3(b)], for all of the five Ca-compounds investigated, a second emitting center is observed, exhibiting a broadband emission assigned to a 5*d* emission. For Ca_{0.65}La_{0.35}F_{2.35} and Na_{0.8}Ca_{0.8}La_{1.2}F₆, this emission is barely seen. We tentatively assign the center exhibiting a photon cascade emission to a Pr³⁺ ion substituted for the trivalent rare-earth-ion site in the lattices. The center exhibiting the 5*d* emission is tentatively assigned to the substitution of the Ca²⁺ site in the lattices. Its occupation is less probable than the substitution of the trivalent Y, La, or Lu sites, and this explains the low photon fluxes observed for the 5*d* emission, despite the fact that they are electric-dipole allowed and supposed to be strong. The temperature dependence of the emission spectrum was also investigated (except for Na_{0.8}Ca_{0.8}La_{1.2}F₆) [see Figs. 4(a)–4(d)]. Besides a thermal broadening of the 4*f* transition bands, the emission spectra at 10 K and at room temperature were nearly unchanged. Thus, a thermal coupling between the emitting centers was

excluded. This also supported the assignment of two independent Pr³⁺ centers in these materials. The different decay characteristic of the emission at different wavelengths is shown in Fig. 5 for Pr³⁺:Ca_{0.9}Y_{0.1}F_{2.1} for wavelengths of 220 nm (pure 5*d* emission) and 250 nm (mixed 5*d* and ¹S₀ emission). Under VUV excitation at 190 nm, the decay at 220 nm was single exponential with a decay time of about 20 ns, whereas the decay at 250 nm could be fitted with a double exponential decay function with approximately 20-ns and 3000-ns decay times. These decay times matched the expected decay times for a 4*f*5*d* → 4*f*² and ¹S₀ → 4*f*² transition.

C. Sr compounds

The overview emission spectra of the Sr compounds investigated, i.e., SrYF₅, Sr_{0.69}La_{0.31}F_{2.31}, and SrF₂ (for comparison), are shown in Fig. 6(a). For SrYF₅ and Sr_{0.69}La_{0.31}F_{2.31} emission transitions from the ¹S₀ level as well as from the ³P₀ level are clearly observed, indicating photon cascade emission. Looking in detail into the short-wavelength spectra [see Fig. 6(b)] all of the Sr compounds investigated exhibit a second emitting center with a broad-

TABLE II. Effective ionic radii in fluorine coordination (from Ref. 16). *: estimated from the value for La.

Ion	Coordination						
	4	6	7	8	9	10	12
Li	0.73	0.88					
Na	1.13	1.16	1.27	1.30	1.46		
K		1.52	1.60	1.65	1.69	1.73	1.74
Rb		1.63	1.70	1.74		1.80	1.87
Mg	0.72	0.86		1.03			
Ca		1.14	1.21	1.26	1.32	1.42	1.49
Sr		1.27	1.55	1.39		1.46	1.54
Ba		1.50	1.53	1.56	1.61	1.66	1.74
Sc		0.89		1.01			
Y				1.16	1.24		
La		1.19	1.24	1.32	1.34	1.42	1.46
Lu		1.00		1.11			
Pr		1.14		1.28	1.32*		

band emission assigned to a $5d$ emission. For $\text{Sr}_{0.69}\text{La}_{0.31}\text{F}_{2.31}$, this emission is barely seen, as in the case of $\text{Ca}_{0.65}\text{La}_{0.35}\text{F}_{2.35}$. We tentatively assign the center exhibiting photon cascade emission to a Pr^{3+} ion substituted for the trivalent rare-earth-ion site in the lattices. The center exhibiting $5d$ emission is tentatively assigned to the substitution of

the Sr^{2+} site in the lattices. As for the Ca compounds, the occupation was less probable than the substitution of the trivalent Y, La, or Lu site, and this explains the low photon fluxes observed for the $5d$ emission. It should be noted that for SrYF_5 crystal data were not available, thus the structure of this compound is not clear. A structure analysis gave no

TABLE III. $\eta_{\text{vis}}^{\text{high}}$, $\eta_{\text{vis}}^{\text{low}}$, and $\eta_{\text{vis},JO}$: quantum efficiencies; Pr PCE site: substituted site with cascade emission; R_{eff} : effective ligand distance [defined as $R_{\text{eff}}=R_i-0.6 \Delta R$ (Ref. 33), where R_i is the ligand distance (Ref. 34) and ΔR is the difference between the ionic radius of Pr^{3+} and the cation, which is substituted]; $R_{2\text{nd}}$: ionic radius of the 2nd cation (Ref. 16); CN : coordination number of the lattice site substituted by the Pr^{3+} ion (Ref. 34); Pr $5d$ site: substituted site with broadband emission. NA indicates that a determination of $\eta_{\text{vis},JO}$ is not possible, because thermal coupling as well as a second optical center is observed. “?” indicates a tentative assignment.

No.	Compound	$\eta_{\text{vis}}^{\text{high}}$	$\eta_{\text{vis},JO}^{\text{low}}$	$\eta_{\text{vis},JO}$	Pr PCE site	$R_{2\text{nd}}(\text{\AA})$	$R_{\text{eff}}(\text{\AA})$	CN	Pr $5d$ site
1	YF_3	1.59	1.59	1.59	Y	1.24	2.27	9	
2	NaYF_4	1.43	1.43	1.43	Y	1.30	2.30	8	
3	LaF_3	1.45	1.45	1.45	La	1.34	2.44	9	
4	NaLaF_4	1.46	1.46	1.46	La	1.16	2.44	8	
5	LuF_3	1.59	1.59	1.59	Lu	1.11	2.16	8	
6	KMgF_3	1.29	1.29	1.29	K	0.86	2.98	12	
7	BaMgF_4	1.30	1.30	1.30	Ba	0.86	2.93	8	
8	PrF_3	1.23	1.23	1.23	Pr	1.29	2.64	9	
9	$\text{Ca}_{0.9}\text{Y}_{0.1}\text{F}_{2.1}$	1.46	1.15	1.46	Y	1.26	2.10	8	Ca
10	$\text{Na}_{0.9}\text{Ca}_{0.9}\text{Y}_{1.1}\text{F}_6$	1.32	0.68	1.32	Y	1.39	2.31	9	Ca
11	$\text{Ca}_{0.65}\text{La}_{0.35}\text{F}_{2.35}$	1.38	1.23	1.38	La	1.26	2.37	8	Ca
12	$\text{Na}_{0.8}\text{Ca}_{0.8}\text{La}_{1.2}\text{F}_6$	1.26	1.04	1.26	La	1.39	2.36	9	Ca
13	$\text{Ca}_{2.028}\text{Lu}_{0.972}\text{F}_7$	1.44	0.98	1.44	Lu	1.26	2.22	8	Ca
14	SrYF_5	1.22	0.75	NA	Y	1.39	2.25	8	Sr
15	$\text{Sr}_{0.69}\text{La}_{0.31}\text{F}_{2.31}$	1.11	0.98	1.11	La	1.39	2.56	8	Sr
16	$\text{Ba}_4\text{Y}_3\text{F}_{17}$	1.67	0.74	NA	Ba?	1.24		8	Y?
17	$\text{Ba}_{0.5}\text{La}_{0.5}\text{F}_{2.5}$	1.39	0.64	NA	Ba?	1.34		8	La?
18	Rb_3YF_6	1.47	0.67	NA	Rb?	1.00		8	Y?
19	$\text{RbLu}_3\text{F}_{10}$	1.34	0.94	1.34	Rb?	1.00		8	Lu?

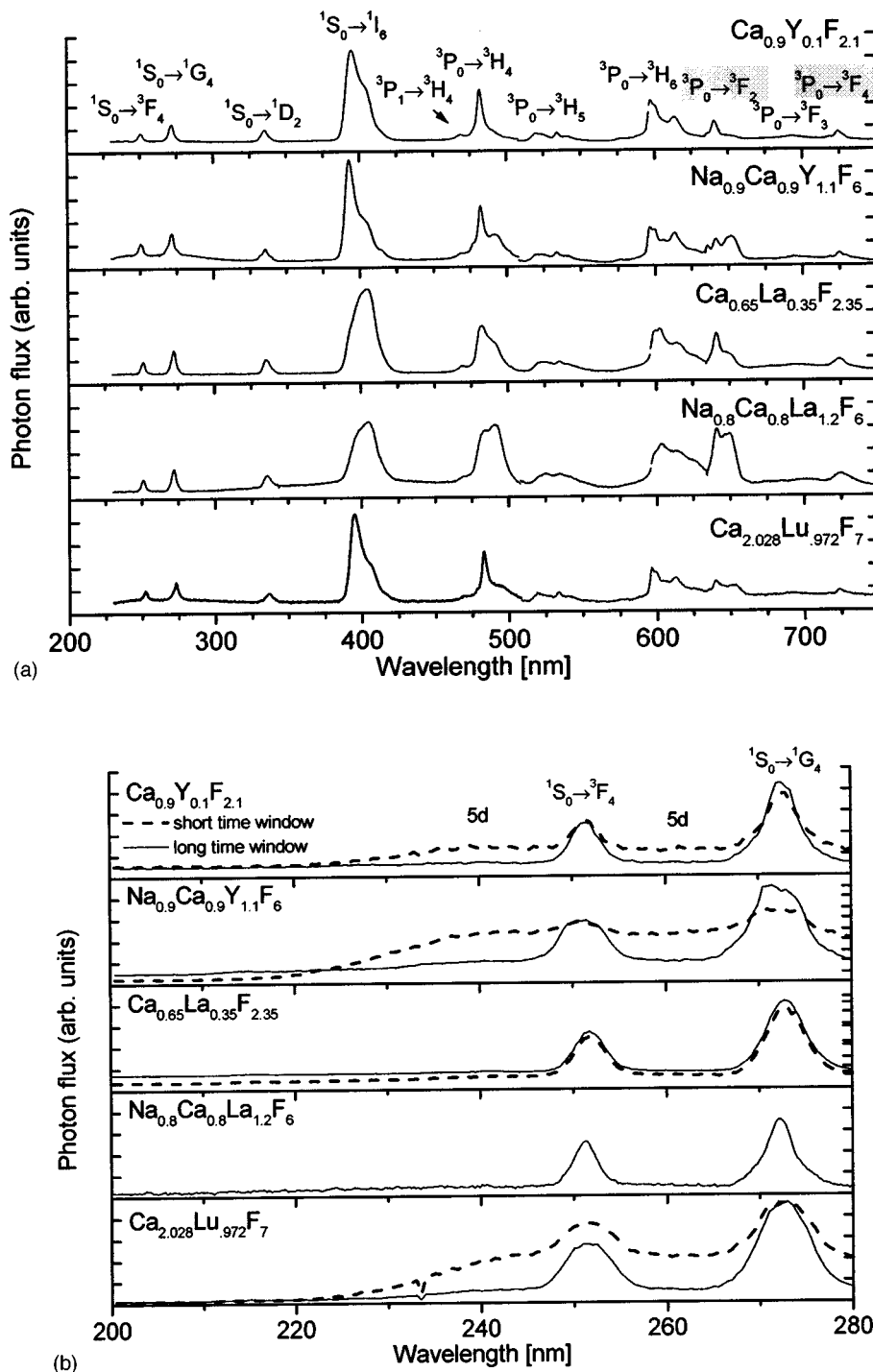


FIG. 3. Room-temperature emission spectra (uncorrected) under excitation at approximately 190 nm of the Ca compounds $\text{Ca}_{0.9}\text{Y}_{0.1}\text{F}_{2.1}$, $\text{Na}_{0.9}\text{Ca}_{0.9}\text{Y}_{1.1}\text{F}_6$, $\text{Ca}_{0.65}\text{La}_{0.35}\text{F}_{2.35}$, $\text{Na}_{0.8}\text{Ca}_{0.8}\text{La}_{1.2}\text{F}_6$, and $\text{Ca}_{2.028}\text{Lu}_{.972}\text{F}_7$. (a) 200 nm–750 nm (CCD camera). (b) 200 nm–280 nm [photomultiplier, except for $\text{Na}_{0.8}\text{Ca}_{0.8}\text{La}_{1.2}\text{F}_6$ (here also CCD)].

clear result; however, a decomposition into SrF_2 and YF_3 was also not observed in the structure analysis. Also the observed emission spectra do not look like the spectra of YF_3 or SrF_2 [see Figs. 2(a) and 2(b) and Figs. 6(a) and 6(b)]. Therefore, we tentatively refer to this compound as SrYF_5 throughout this manuscript. The temperature dependence of the emission spectrum was also investigated [see Figs. 6(c) and 6(d)]. For SrYF_5 an increase in the $5d$ emission bands compared to the 1S_0 emission bands was observed with increasing temperature, indicating a thermally activated $5d$ emission for the center exhibiting cascade emission. The different decay characteristic of the emission at different wave-

lengths for $\text{Pr}^{3+}:\text{SrYF}_5$ is shown in Fig. 7(a) for wavelengths of 240 nm (pure $5d$ emission) and 252 nm (mixed $5d$ and 1S_0 emission) under VUV excitation at 190 nm, giving a single exponential with a decay time of about 25 ns and a double exponential decay with decay times of 25 ns and 250 ns, respectively. These decay times are also in agreement with the expected values.

For $\text{Sr}_{0.69}\text{La}_{0.31}\text{F}_{2.31}$ the emission spectra at 10 K and at room temperature were nearly unchanged. As for the Ca compounds, a thermal coupling between the emitting centers could be excluded. The decay characteristic is shown in Fig. 7(b), exhibiting a double exponential decay of approximately

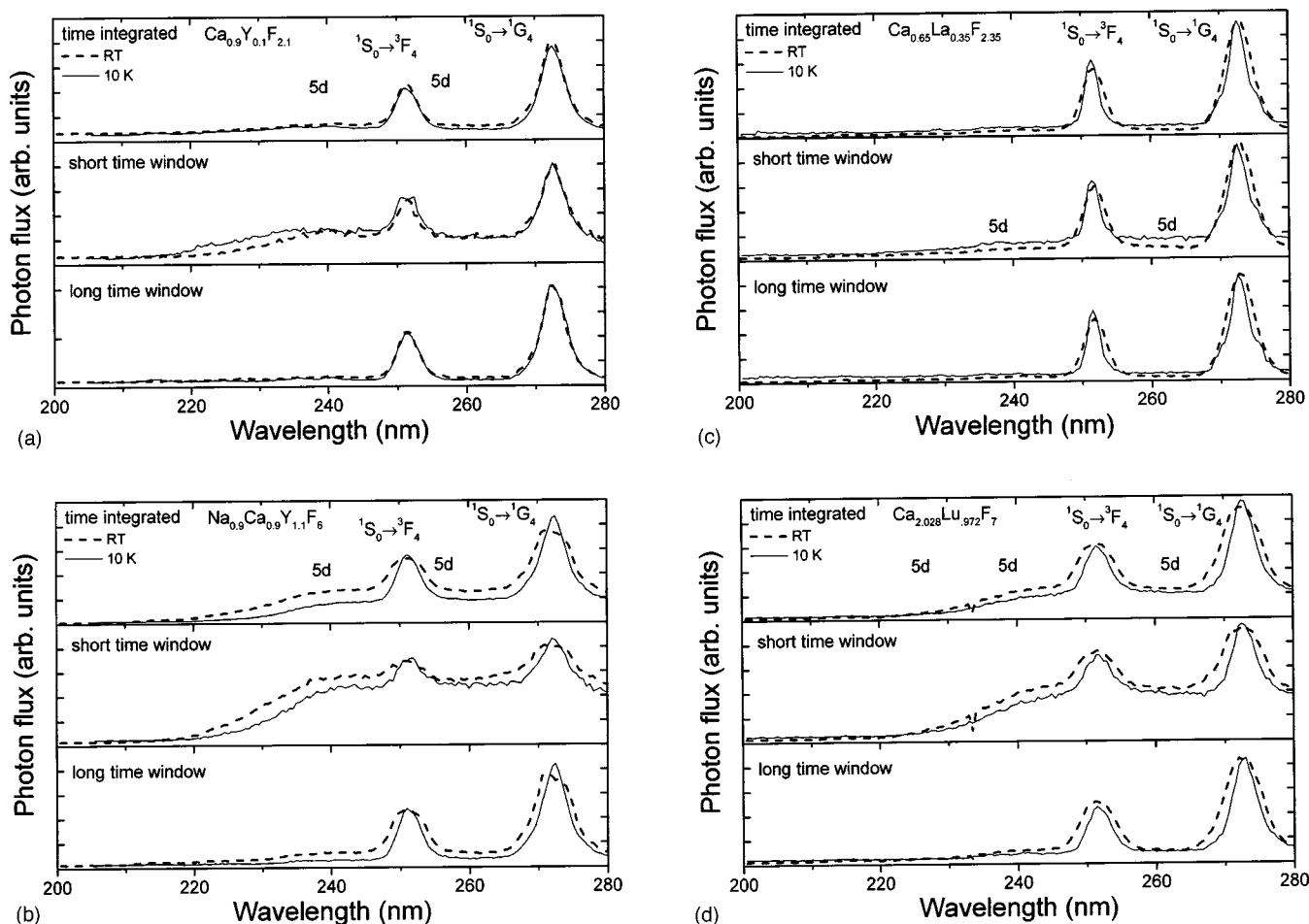


FIG. 4. Emission spectra of the Ca compounds (uncorrected) under excitation at approximately 190 nm at room temperature and at 10 K for different time windows of the photomultiplier. (a) $\text{Ca}_{0.9}\text{Y}_{0.1}\text{F}_{2.1}$. (b) $\text{Na}_{0.9}\text{Ca}_{0.9}\text{Y}_{1.1}\text{F}_6$. (c) $\text{Ca}_{0.65}\text{La}_{0.35}\text{F}_{2.35}$. (d) $\text{Ca}_{2.028}\text{Lu}_{.972}\text{F}_7$.

20 ns and 500 ns. This observation supports the assignment of two independent Pr^{3+} centers in this material.

D. Ba compounds

The overview emission spectra of the Pr^{3+} -doped Ba compounds investigated, i.e., $\text{Ba}_4\text{Y}_3\text{F}_{17}$ and $\text{Ba}_{0.5}\text{La}_{0.5}\text{F}_{2.5}$, are

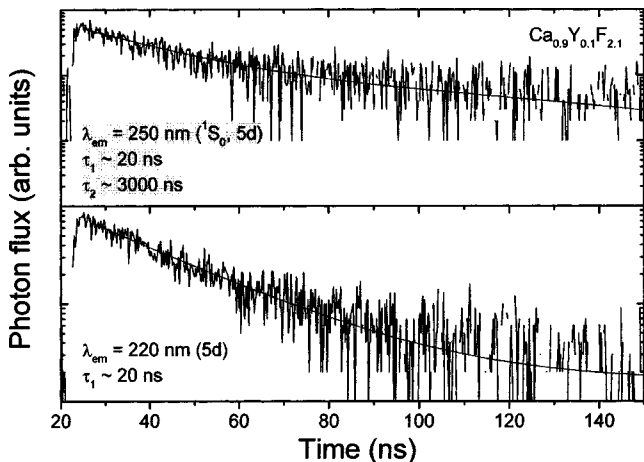


FIG. 5. Decay characteristics at 10 K of $\text{Pr}^{3+}:\text{Ca}_{0.9}\text{Y}_{0.1}\text{F}_{2.1}$ at different monitoring wavelengths.

shown in Fig. 8(a). For both compounds, emission transitions from the 1S_0 level as well as from the 3P_0 level are clearly observed, indicating photon cascade emission. Looking in detail into the short-wavelength spectra [see Fig. 8(b)], the Ba compounds also exhibit broadband emissions assigned to $5d$ emissions.

For $\text{Ba}_4\text{Y}_3\text{F}_{17}$ the low-temperature emission spectra of the short-time and long-time windows are different [see Fig. 9(a)]. Thus two optical centers are identified. However, the room-temperature emission spectra of the short-time and long-time windows are very similar [see Figs. 8(b) and 9(a)]. Furthermore, the short-time window spectra at low and room temperatures are similar, whereas the long-time window spectra differ significantly [see Fig. 9(a)]. Thus we conclude that in $\text{Ba}_4\text{Y}_3\text{F}_{17}$ the Pr^{3+} ion occupies two different centers, one emitting from the $5d$ level, and the other emitting from the 1S_0 level at low temperatures. At room temperatures, a thermal occupation of the $5d$ levels of the latter center occurs, yielding a mixed 1S_0 and $5d$ emission. The room-temperature decay characteristics of $\text{Pr}^{3+}:\text{Ba}_4\text{Y}_3\text{F}_{17}$ under excitation at 190 nm at monitoring wavelengths of 272 nm (upper trace) and 220 nm (lower trace) are shown in Fig. 10. Both decays are single exponential, however, with short, but different decay times. These observations support the assignment of two centers, one being purely $5d$ emitting, and the

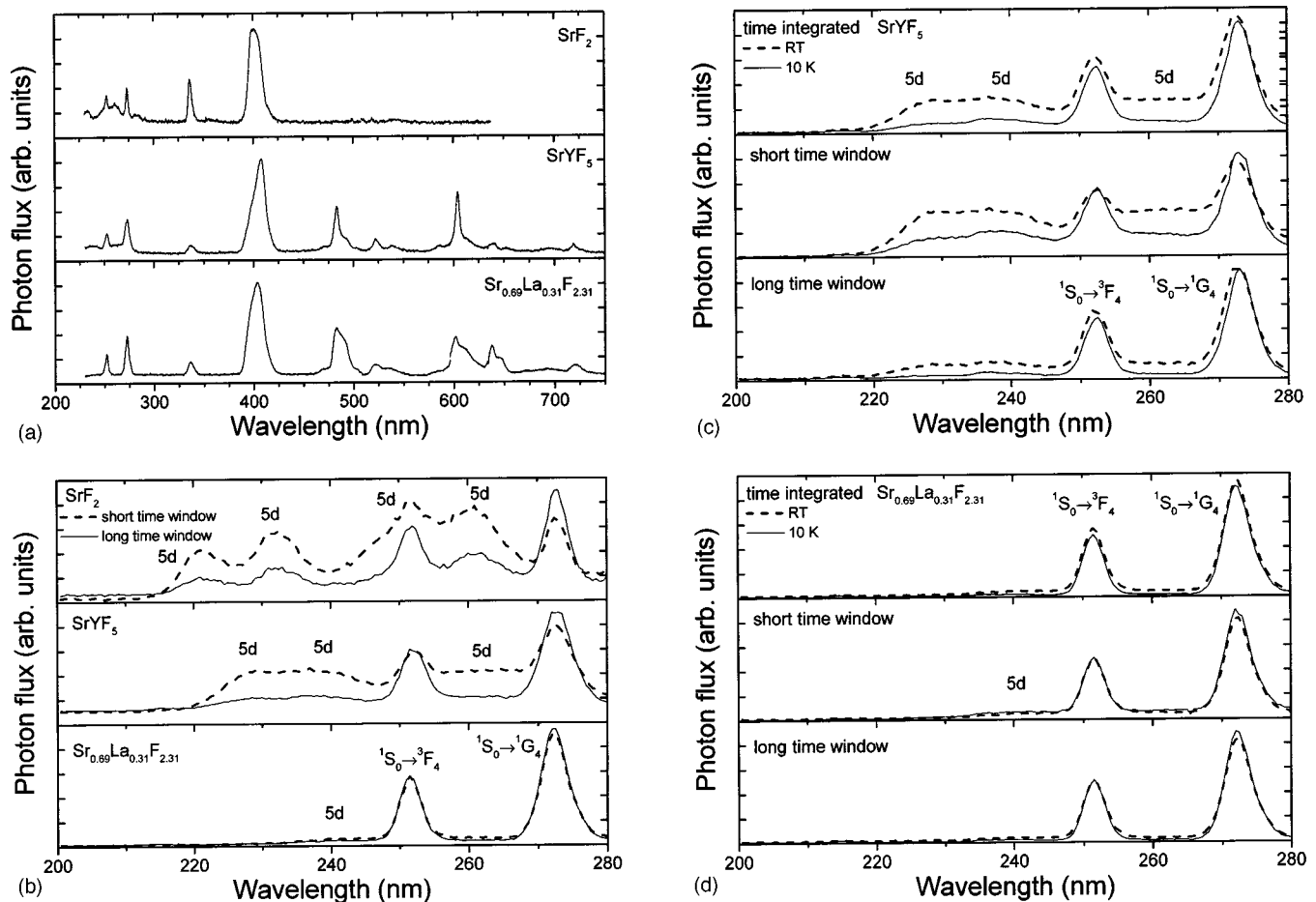


FIG. 6. (a) Room-temperature emission spectra of SrF_2 , SrYF_5 , and $\text{Sr}_{0.69}\text{La}_{0.31}\text{F}_{2.31}$. Besides the cascade emission, also broadband emission from the $4f5d$ level is observed. (b) Room-temperature emission spectra between 200 nm and 280 nm for different time windows of the photomultiplier. For SrYF_5 and SrF_2 two different centers are observed. (c) Emission spectra of SrYF_5 at room temperature and at 10 K for different time windows of the photomultiplier. For SrYF_5 thermal coupling is observed. (d) Emission spectra of $\text{Sr}_{0.69}\text{La}_{0.31}\text{F}_{2.31}$ at room temperature and at 10 K for different time windows of the photomultiplier. For $\text{Sr}_{0.69}\text{La}_{0.31}\text{F}_{2.31}$ a weak second optical center is observed. All spectra are not corrected for the monochromator-detector responsivity, and they were measured under excitation at approximately 190 nm.

other being thermally activated, leading also to a small decay time. From the consideration of the ionic radii of the second cation, the effective ligand distance, and the coordination numbers in this compound (see Table III) we further conclude that the $5d$ emission occurs from Pr^{3+} ions on the Y site, e.g., in BaY_2F_8 , where the Pr^{3+} ion enters solely the Y site, $5d$ emission is also observed (see Fig. 8). The thermally coupled $4f^2$ and $4f5d$ emissions occur from Pr^{3+} ions on the Ba lattice site, e.g., for BaMgF_4 and BaSiF_6 cascade emission is also observed.^{9,18}

For $\text{Ba}_{0.5}\text{La}_{0.5}\text{F}_{2.5}$ similar observations are made [see Figs. 8(b) and 9(b)]. Also here it was assumed that the Pr^{3+} ion substitutes at both the rare-earth-ion site as well as the Ba site. The Ba site exhibited pure 1S_0 emission at 10 K and mixed 1S_0 and $5d$ emission at room temperature, whereas the Pr^{3+} ion on the La site exhibited $5d$ emission.

E. Rb compounds

The overview emission spectra of the Pr^{3+} -doped Rb compounds investigated, i.e., Rb_3YF_6 and $\text{RbLu}_3\text{F}_{10}$, are shown

in Fig. 11(a). For Pr^{3+} -doped Rb_3YF_6 emission transitions both from the 1S_0 level as well as from the 3P_0 level are clearly observed, whereas for Pr^{3+} -doped $\text{RbLu}_3\text{F}_{10}$, the emission from the 3P_0 level is rather weak. Both compounds are cascade emitters. Looking in detail into the short-wavelength spectra [see Fig. 11(b)] both compounds also exhibit broadband emission assigned to a $5d$ emission. For $\text{RbLu}_3\text{F}_{10}$ the room-temperature emission spectra of the long-time and short-time windows are very different, thus two optical centers are present in this compound. The room-temperature decay curves [shown in Fig. 12(b)] also support this assumption. Furthermore, we assume that the cascade emission might be caused by the substitution of the Rb site in the lattice, which has a high coordination number and a large ionic radius. The Pr^{3+} ions substituting in the Lu site are assumed to emit from the $5d$ levels. For Rb_3YF_6 , the situation is somewhat different. Here also in the long-time window emission-spectrum broadband emission bands are observed. Thus we tentatively conclude that two optical centers are present in Rb_3YF_6 . The room-temperature decay charac-

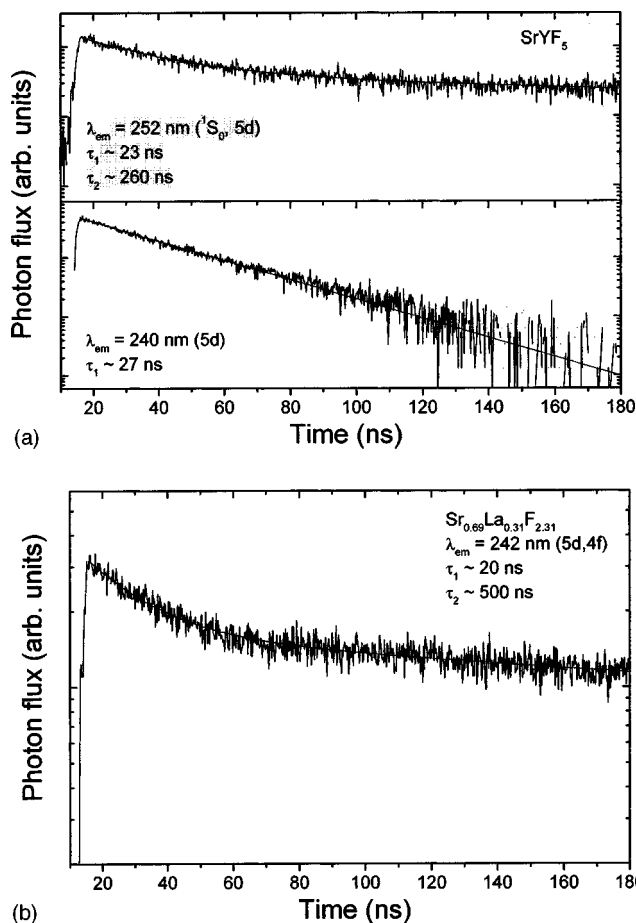


FIG. 7. (a) Room-temperature decay characteristics of $\text{Pr}^{3+}:\text{SrYF}_5$ at different monitoring wavelengths. (b) Room-temperature decay characteristics of $\text{Pr}^{3+}:\text{Sr}_{0.69}\text{La}_{0.31}\text{F}_{2.31}$ at 242 nm, indicating the double exponential decay. All decay curves were measured under excitation at approximately 190 nm.

teristics of $\text{Pr}^{3+}:\text{Rb}_3\text{YF}_6$ for different monitoring wavelengths are shown in Fig. 12(a). They also indicate two optical centers with relative short, but single exponential lifetimes. One center exhibits solely a $5d$ emission, and we tentatively assign this center to Pr^{3+} ions on the Y^{3+} lattice site, while the other exhibits a mixed ${}^1S_0/5d$ emission and is tentatively assigned to Pr^{3+} ions substituting in the Rb^+ lattice site. However, for a clearer analysis, low-temperature-measurements spectra would be necessary.

In summary, we have found in the compounds investigated several different types of emission transitions. These are pure cascade emitters, compounds exhibiting cascade emission as well as broadband $5d$ emission due to two optical centers, and compounds exhibiting cascade emission with a thermally activated $5d$ emission as well as a pure $5d$ emission also, due to two optical centers. In Table I a summary of the different types of emissions for the compounds investigated is given.

V. SPECTROSCOPIC RESULTS—EXCITATION

For possible application in Xe-discharge lamps, it is required that the potential phosphors exhibit a strong absorp-

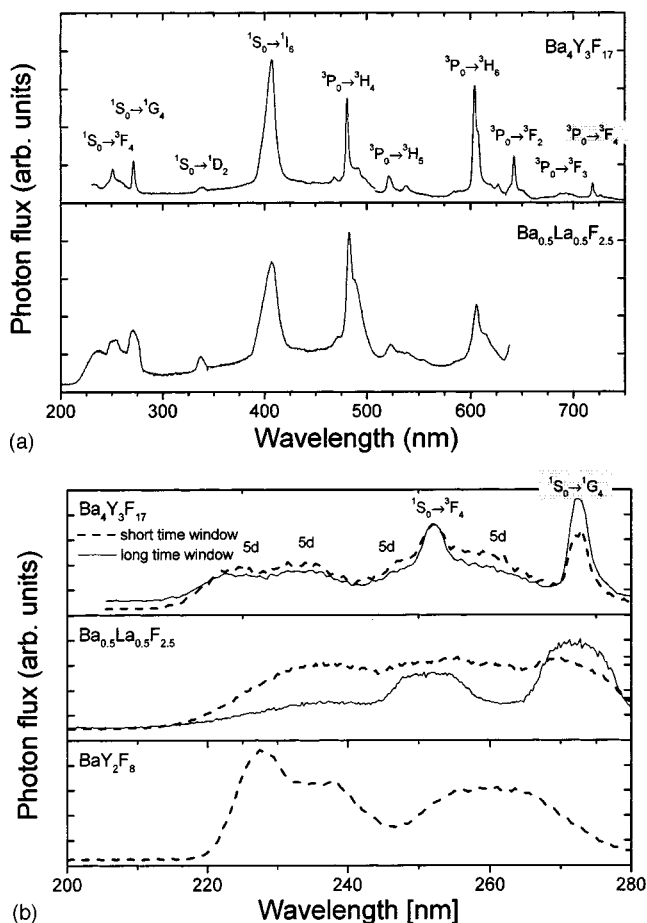
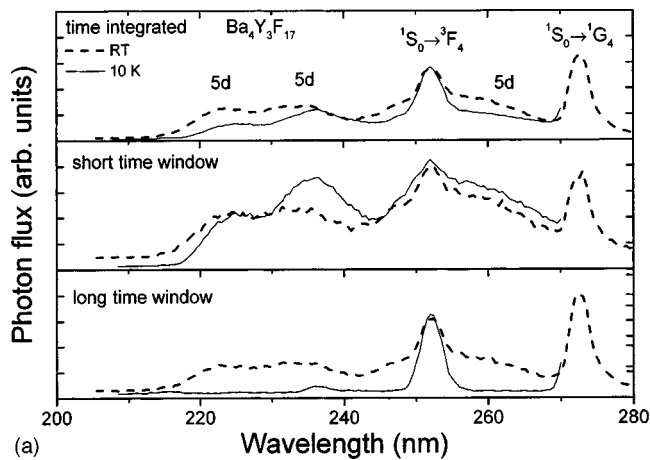
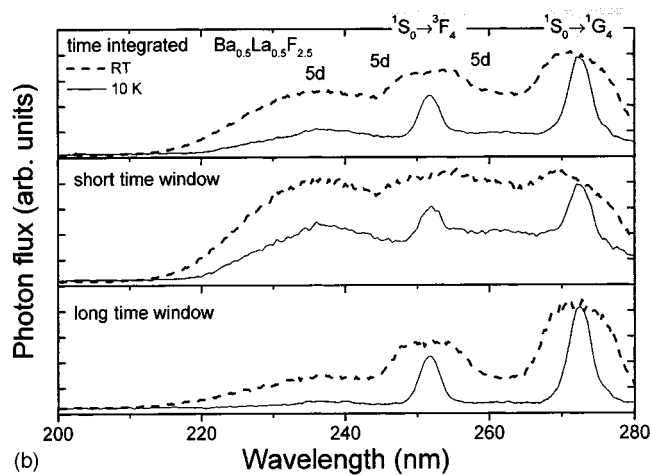


FIG. 8. (a) Room-temperature emission spectra (200 nm–750 nm, uncorrected) of the Ba compounds investigated. (b) Room-temperature emission spectra (uncorrected) between 200 nm and 280 nm for different time windows of the photomultiplier. For comparison, the emission spectrum of BaY_2F_8 is also shown. All spectra were measured under excitation at approximately 190 nm.

tion band in the spectral region of the Xe-discharge, which spans approximately between 140 nm and 185 nm with two peaks at approximately 150 nm and 170 nm.¹⁹ The excitation spectra for the ${}^1S_0 \rightarrow {}^1I_6$ emission band around 400 nm are shown in Fig. 13 for the compounds investigated. Most of the materials have a strong excitation band between 180 nm and 200 nm belonging to the ${}^3H_4 \rightarrow 4f5d$ bands. These transitions are parity allowed and thus very strong, as can be seen from the comparison with the ${}^3H_4 \rightarrow {}^1S_0$ excitation line around 215 nm. Although these main excitation bands are at somewhat too long wavelengths for an ideal excitation with the Xe-discharge, some of the materials also at least exhibit excitation bands in the spectral region of the Xe-emission. For a detailed analysis of the excitation bands, low-temperature spectra and high-resolution spectroscopy would be necessary, which are beyond the scope of this work. Thus, only a basic analysis of the excitation spectra will be given in the following. In general, for a $4f5d$ configuration 140 energy levels are expected to be formed by the product states from the electron in the $4f$ shell (14 states) and the electron in the $5d$ shell (10 states). A basic and very simple interpretation is possible in terms of a strong field assignment.^{20,21}



(a)



(b)

FIG. 9. (a) Emission spectra (uncorrected) of $\text{Ba}_4\text{Y}_3\text{F}_{17}$ at room temperature and at 10 K for different time windows of the photomultiplier. (b) Emission spectra (uncorrected) of $\text{Ba}_{0.5}\text{La}_{0.5}\text{F}_{2.5}$ at room temperature and at 10 K for different time windows of the photomultiplier. All spectra were measured under excitation at approximately 190 nm.

The assignments of the observed bands are based on the assumption that the major contribution to the energy-level splitting originates from the orbital splitting of the $5d$ electron states of the Pr^{3+} ion. Thus, two groups of bands can be assigned, consisting of the two bands of the $4f^*5d(e_g)$ states and the energetically higher group of three bands of the $4f^*5d(t_{2g})$ states, giving in total five broadbands sorted into two groups. This can be observed for YF_3 , LuF_3 , LaF_3 , and KMgF_3 rather clearly, but for the other compounds only barely. Further splitting of these bands occurs due to the spin-orbit interactions of the $4f$ electron and due to crystal-field splitting. In most of the excitation spectra for the compounds investigated we also observe the ${}^3H_4 \rightarrow {}^1S_0$ excitation line on the long-wavelength side of the ${}^3H_4 \rightarrow 4f5d$ excitation bands. This indicates that in these materials the 1S_0 level is below the $4f5d$ levels, giving rise to cascade emission.

In the excitation spectra of $\text{Ba}_4\text{Y}_3\text{F}_{17}$, Rb_3YF_6 , and $\text{RbLu}_3\text{F}_{10}$ (see also Fig. 13) the second optical center is also clearly observed. The monitoring wavelengths were 235 nm, 230 nm, and 311 nm, respectively, i.e., at wavelengths where the $5d$ emission occurs (see also the discussion in Sec. IV).

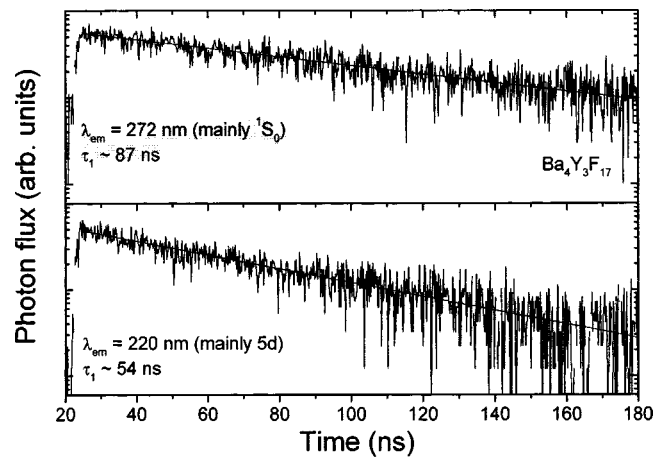


FIG. 10. Room-temperature decay characteristics of $\text{Pr}^{3+}:\text{Ba}_4\text{Y}_3\text{F}_{17}$ at monitoring wavelengths of 272 nm (upper trace) and 220 nm (lower trace). All decay curves were measured under excitation at approximately 190 nm.

This observation supports the assignment and conclusion in the previous section concerning the different Pr^{3+} centers. It should be noted that excitation measurements of the second emission center were not performed for all compounds.

VI. SPECTROSCOPIC RESULTS—QUANTUM EFFICIENCY

For a potential use as a lamp phosphor, the quantum efficiency of the emission is one of the most important parameters besides absorption efficiency, emission wavelength, stability, and production costs. Thus at the beginning of this section we would like to introduce and define the different types of quantum efficiencies used in the following. These are in specific

(i) external quantum efficiency: η_{ext} = the number of emitted photons in the visible spectral range divided by the number of excitation photons. This is the value that is most important for applications; it contains the absorption efficiency and, if observed for a long time, also the stability of a phosphor.

(ii) internal quantum efficiency: η_{int} = the number of emitted photons in the visible spectral range divided by the number of ions in the 1S_0 level. This value excludes the absorption efficiency and thus characterizes only the efficiency of the emission. The long-term stability can be observed.

(iii) internal theoretical quantum efficiency: $\eta_{\text{vis},JO}$ = the number of emitted photons in the visible spectral range, calculated by the Judd-Ofelt theory divided by the number of ions in the 1S_0 level (see the details below). This value characterizes only the efficiency of the emission by measuring the emission from the 1S_0 level. The long-term stability cannot be observed.

(iv) internal approximated quantum efficiency: $\eta_{\text{vis},\beta}$ = the number of emitted photons in the visible spectral range, estimated by the measured branching ratio of the ${}^1S_0 \rightarrow {}^1I_6$ transition divided by the number of ions in the 1S_0 level. This value characterizes only the efficiency of the emission by

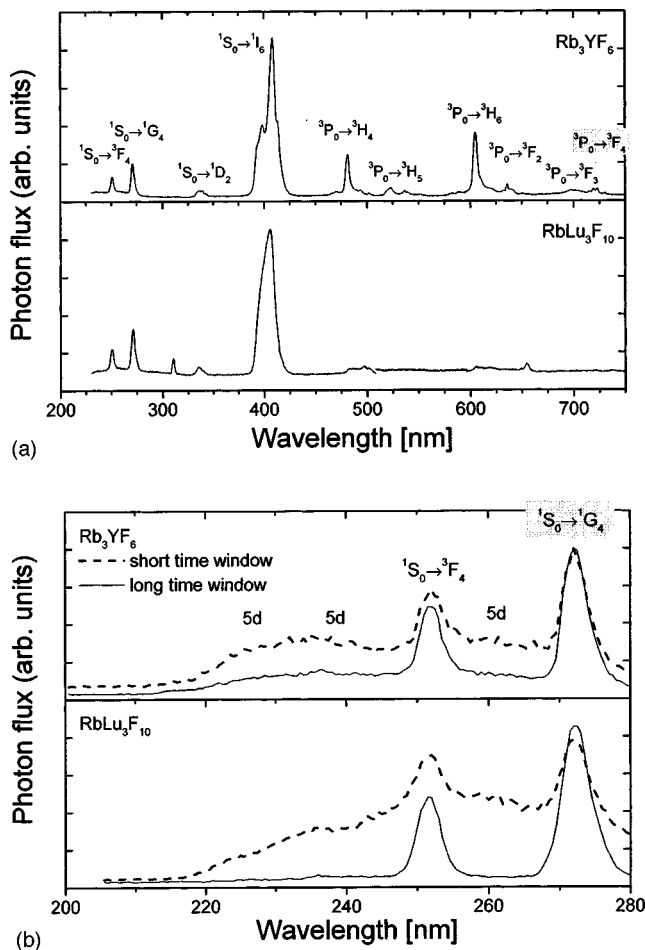


FIG. 11. (a) Room-temperature emission spectra (200 nm–750 nm, uncorrected) of the Rb compounds investigated. (b) Emission spectra (uncorrected) between 200 nm and 280 nm for different time windows of the photomultiplier. For all materials two different centers are observed. All spectra were measured under excitation at approximately 190 nm.

measuring the emission from the 1S_0 level. The long-term stability cannot be observed.

The external quantum efficiency η_{ext} for the visible light of a luminescent material can in principle be determined experimentally, but due to experimental difficulties, especially in the VUV range, this is not an easy and thus not a common procedure. Furthermore, especially in the first stages of the development of a new compound, the measurements might be disturbed by impurities in and contamination (e.g., oxygen) of the compounds. Thus, attempts to predict η_{ext} for Pr^{3+} -doped materials by applying the Judd-Ofelt theory^{22–24} were made already in the 1970s.^{5,25} If one takes into account the reduced matrix elements $\|U\|^2$ and the oscillator strengths for all transitions involved in the photon cascade emission process, it follows that the ratios between the phenomenologically determined Judd-Ofelt parameters Ω_2/Ω_6 and Ω_4/Ω_6 determine the value for the internal theoretical quantum efficiency $\eta_{\text{vis},JO}$, which is considered to be a good estimate for η_{ext} . These Ω_2/Ω_6 and Ω_4/Ω_6 ratios can be determined by a fit to the experimentally observed branching ratios of the 1S_0 emission transitions (see e.g., Refs. 6, 9, and

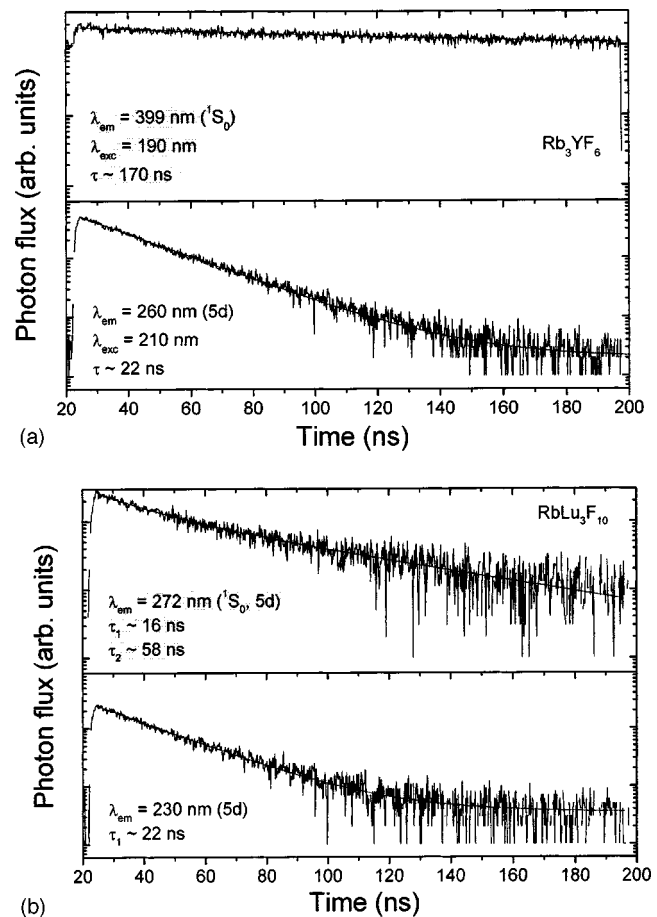


FIG. 12. Room-temperature decay characteristics of (a) $\text{Pr}^{3+}:\text{Rb}_3\text{YF}_6$ (excitation wavelengths at 190 nm and 210 nm) and (b) $\text{Pr}^{3+}:\text{RbLu}_3\text{F}_{10}$ (excitation wavelength at 190 nm) at different monitoring wavelengths.

10). The smaller these ratios are, the higher is the probability for the $^1S_0 \rightarrow ^1I_6$ transition and for transitions from the 3P_0 located in the visible range. In Fig. 14 the visible quantum efficiency $\eta_{\text{vis},JO}$ for different ratios of the Judd-Ofelt parameters Ω_2/Ω_6 and Ω_4/Ω_6 are plotted. It is well known that Judd-Ofelt calculations for the Pr^{3+} ion usually fail. This holds especially for the branching ratios of the transitions from the 3P_0 level and the 3P_0 decay time. It is assumed that the proximity of the $5d$ levels has a strong affect on the transition probabilities and energy-level wavefunctions. Thus the approximations used in the Judd-Ofelt theory are no longer valid (see e.g., Ref. 26). The 1S_0 is energetically very close to the $5d$ levels, and therefore an even stronger influence of the $5d$ levels on this level is expected. The validity of the Judd-Ofelt calculations are therefore, of course, also questionable. However, the calculation based on the above-described fitting procedure describes the experimentally observed branching ratios very well. Furthermore almost all transitions from the $^3P_{0,1}$ levels occur in the visible spectral range. Thus the calculated values for the internal theoretical quantum efficiency $\eta_{\text{vis},JO}$ are expected to be rather reasonable, as will be seen in the discussion below.

However, before the determination of the branching ratios and the following Judd-Ofelt calculations can be performed,

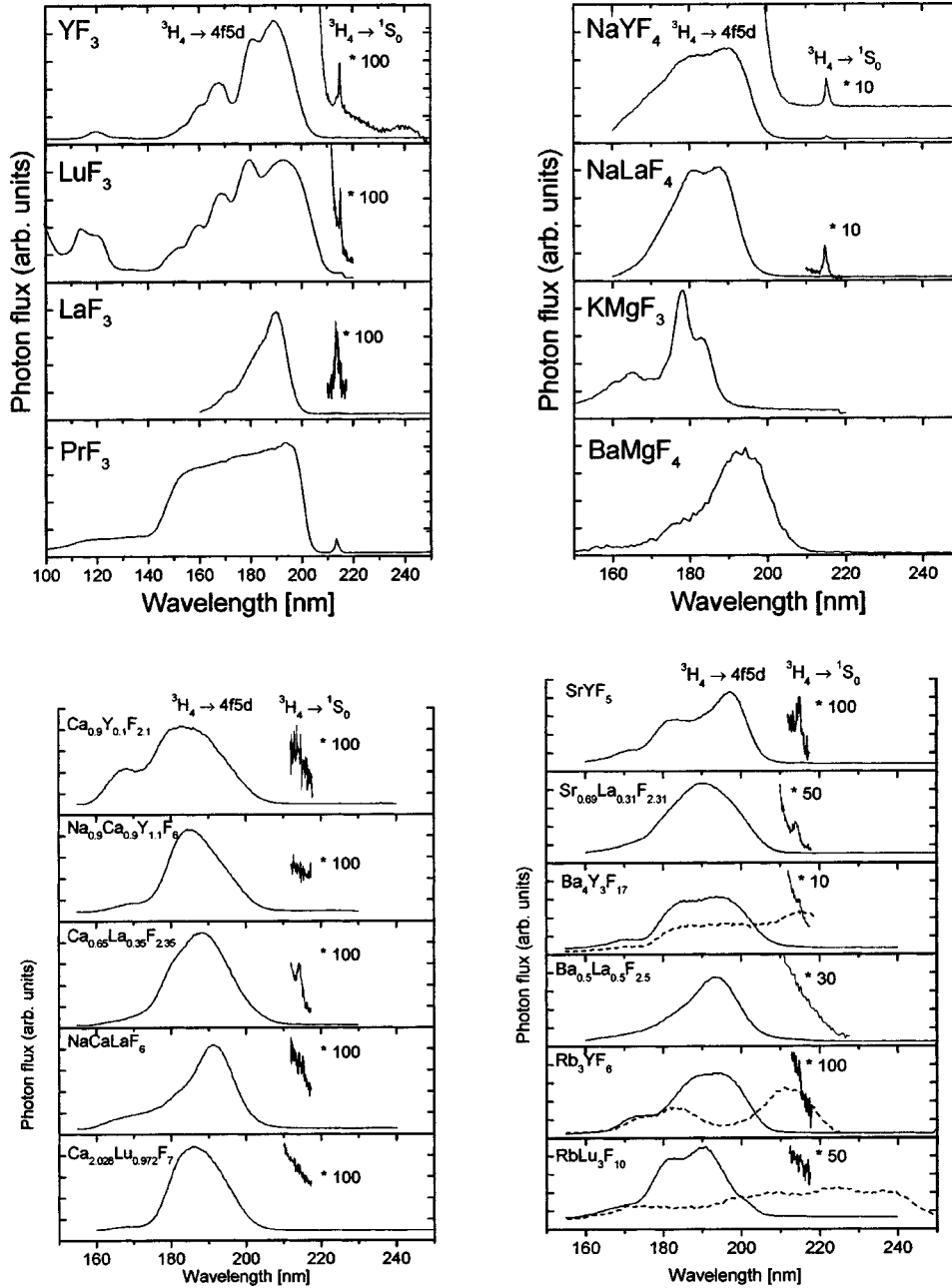


FIG. 13. Room-temperature excitation spectra (uncorrected) of the compounds investigated. Resolution approximately 0.3 nm. Solid lines: Monitoring wavelength λ_{em} approximately 400 nm ($^1S_0 \rightarrow ^1I_6$). Dashed lines: Excitation spectra of second emitting center for $\lambda_{em} = 235$ nm ($Ba_4Y_3F_{17}$), $\lambda_{em} = 230$ nm (Rb_3YF_6), and $\lambda_{em} = 311$ nm ($RbLu_3F_{10}$).

one has not only to perform the correction procedure concerning the spectral responsivity of the setup (“spectral correction”—see section III). It is also necessary to take into account the emission bands in the spectra, which are not due to the 1S_0 transitions, e.g., $5d-4f$ transitions from the same or a different center, charge-transfer transitions, and host-correlated transitions, which overlap with the 1S_0 transitions. These additional emission bands have to be deducted first from the measured emission spectrum in order to obtain the pure 1S_0 emission transitions for the correct determination of their branching ratios (“band correction”).

Applying these correction procedures to the materials investigated, we obtain the Judd-Ofelt parameters and quantum efficiencies $\eta_{vis,JO}^{high}$ listed in Tables III and IV. $\eta_{vis,JO}^{high}$ represents an upper limit for the quantum efficiency. Its value considers only transitions belonging to the cascade, i.e., 1S_0

$\rightarrow ^1I_6$ and $^3P_{0,1} \rightarrow 4f^2$, which are between 380 nm and 750 nm. A lower limit for the quantum efficiency $\eta_{vis,JO}^{low}$ can also be determined by taking into account the above-described additional emissions from different centers or levels as competing processes. Thus $\eta_{vis,JO}^{low} = \beta_{1S_0} \eta_{vis,JO}^{high}$, with β_{1S_0} as the ratio between emissions from the 1S_0 level to all emissions between 200 nm and 450 nm. The values for $\eta_{vis,JO}^{low}$ are also given in Table III. The determination of both values, $\eta_{vis,JO}^{high}$ and $\eta_{vis,JO}^{low}$, makes sense if one considers that for each of the compounds the origins of the additional emissions, their influence on the quantum efficiency of the emission in a specific compound, and the possibility of reducing this influence have to be analyzed in detail. This will be done in the following.

(i) Pure 1S_0 emission. A correction is not necessary and

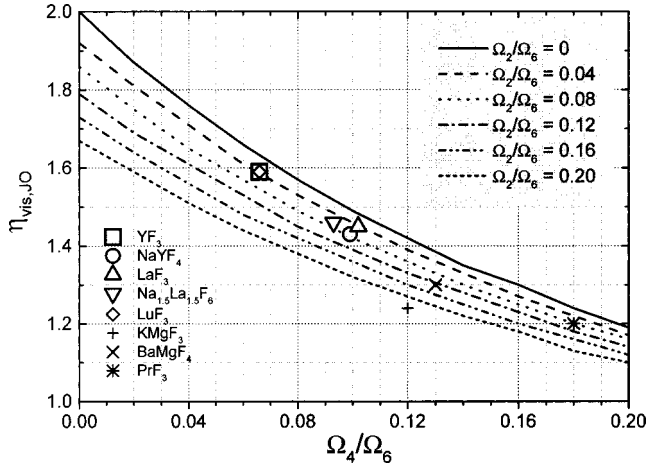


FIG. 14. Calculated visible quantum efficiency $\eta_{\text{vis},JO}$ for different ratios of the Judd-Ofelt parameters Ω_2/Ω_6 and Ω_4/Ω_6 . The values for the pure cascade emitters are also indicated.

$\eta_{\text{vis},JO}$ is equal to $\eta_{\text{vis},JO}^{\text{high}}$. As examples, see the emission spectra shown in Fig. 2 (except for PrF_3).

(ii) Mixed 1S_0 and $5d$ emission with one optical center. The $5d$ levels are energetically just above the S_0 level and these levels are thus thermally coupled. $\eta_{\text{vis},JO}$ is close to $\eta_{\text{vis},JO}^{\text{low}}$, because the $5d$ emissions cannot be avoided at room temperature. From the Pr^{3+} -doped compounds investigated, none exhibits this type of emission.

(iii) Mixed 1S_0 and $5d$ emission with one optical center. The 1S_0 and $5d$ are not thermally coupled. This rare case means that there is a large Huang-Rhys parameter for the $5d$

level, and the emissions from the 1S_0 level and $5d$ levels do not affect each other. A correction is necessary and $\eta_{\text{vis},JO}$ is close to $\eta_{\text{vis},JO}^{\text{low}}$. Within the group of materials investigated here, this case was also not observed.

(iv) Mixed 1S_0 and $5d$ emissions with two centers. The value for $\eta_{\text{vis},JO}$ is estimated to be close to $\eta_{\text{vis},JO}^{\text{high}}$. A substitution of a different host lattice site by the Pr^{3+} ion is assumed, which exhibits $5d$ emission. However, it might be possible to suppress—at least partly—these $5d$ centers from incorporation by the appropriate preparation of the compound. Thus, $\eta_{\text{vis},JO}^{\text{high}}$ describes more accurately the spectroscopic behavior of the center exhibiting cascade emission. Examples discussed in this manuscript are $\text{Ca}_{0.9}\underline{\text{Y}}_{0.1}\text{F}_{2.1}$, $\text{Na}_{0.9}\text{Ca}_{0.9}\underline{\text{Y}}_{1.1}\text{F}_6$, $\text{Ca}_{0.65}\underline{\text{La}}_{0.35}\text{F}_{2.35}$, $\text{Na}_{0.8}\text{Ca}_{0.8}\underline{\text{La}}_{1.2}\text{F}_6$, $\text{Sr}_{0.69}\underline{\text{La}}_{0.31}\text{F}_{2.31}$, $\text{Ca}_{2.028}\underline{\text{Lu}}_{.972}\text{F}_7$, and $\text{Rb}\underline{\text{Lu}}_3\text{F}_{10}$. The underlined ion represents the substituted site, for which $\eta_{\text{vis},JO}$ is determined.

(v) Mixed 1S_0 and host emission. A correction is necessary, because host emission cannot be prevented by preparational procedures. $\eta_{\text{vis},JO}$ is in principle close to $\eta_{\text{vis},JO}^{\text{low}}$ and is the value to be considered for practical applications. However, $\eta_{\text{vis},JO}^{\text{high}}$ should be taken into account for the characteristics of the Pr^{3+} ion itself. As an example, the emission spectrum of PrF_3 is shown in Fig. 2(a), for details of the spectroscopy of PrF_3 see also Refs. 10 and 27–29.

(vi) Mixed 1S_0 and impurity. This situation is similar to case (iv). $\eta_{\text{vis},JO}$ is assumed to be equal to $\eta_{\text{vis},JO}^{\text{high}}$.

(vii) Two optical centers, one exhibiting thermal coupling. Here a determination of $\eta_{\text{vis},JO}$ is not possible, because it is not possible to clearly distinguish between the optical centers. $\eta_{\text{vis},JO}$ is between $\eta_{\text{vis},JO}^{\text{low}}$ and $\eta_{\text{vis},JO}^{\text{high}}$. Some examples

TABLE IV. $\beta(^1S_0 \rightarrow ^1I_6)$: experimentally determined branching ratio of the $^1S_0 \rightarrow ^1I_6$ transition; $\eta_{\text{vis},\beta} := 2\beta(^1S_0 \rightarrow ^1I_6)$: estimated visible quantum efficiency; Ω_2/Ω_6 , Ω_4/Ω_6 : ratios of the Judd-Ofelt parameters; $\eta_{\text{vis},JO}^{\text{high}}$: calculated visible quantum efficiency.

No.	Compound	$\beta(^1S_0 \rightarrow ^1I_6)$	$\eta_{\text{vis},\beta}$	Ω_2/Ω_6	Ω_4/Ω_6	$\eta_{\text{vis},JO}^{\text{high}}$
1	YF_3	0.789	1.578	0.015	0.066	1.59
2	NaYF_4	0.710	1.420	0.024	0.099	1.43
3	LaF_3	0.721	1.442	0.022	0.102	1.45
4	$\text{Na}_{1.5}\text{La}_{1.5}\text{F}_6$	0.727	1.454	0.026	0.093	1.46
5	LuF_3	0.790	1.580	0.014	0.066	1.59
6	KMgF_3	0.625	1.250	0.170	0.120	1.29
7	BaMgF_4	0.591	1.182	0.122	0.129	1.30
8	PrF_3	0.629	1.258	0.025	0.180	1.23
9	$\text{Ca}_{0.9}\text{Y}_{0.1}\text{F}_{2.1}$	0.719	1.438	0.050	0.086	1.46
10	$\text{Na}_{0.9}\text{Ca}_{0.9}\text{Y}_{1.1}\text{F}_6$	0.648	1.296	0.061	0.121	1.32
11	$\text{Ca}_{0.65}\text{La}_{0.35}\text{F}_{2.35}$	0.682	1.364	0.057	0.105	1.38
12	$\text{Na}_{0.8}\text{Ca}_{0.8}\text{La}_{1.2}\text{F}_6$	0.621	1.242	0.066	0.140	1.26
13	$\text{Ca}_{2.028}\text{Lu}_{.972}\text{F}_7$	0.713	1.426	0.045	0.091	1.44
14	SrYF_5	0.607	1.214	0.044	0.164	1.22
15	$\text{Sr}_{0.69}\text{La}_{0.31}\text{F}_{2.31}$	0.550	1.100	0.062	0.200	1.11
16	$\text{Ba}_4\text{Y}_3\text{F}_{17}$	0.827	1.654	0.019	0.047	1.67
17	$\text{Ba}_{0.5}\text{La}_{0.5}\text{F}_{2.5}$	0.682	1.364	0.043	0.106	1.39
18	Rb_3YF_6	0.729	1.458	0.028	0.089	1.47
19	$\text{RbLu}_3\text{F}_{10}$	0.665	1.330	0.028	0.123	1.34

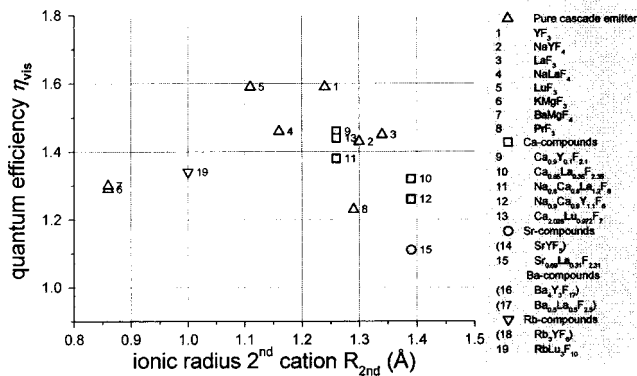


FIG. 15. Quantum efficiency $\eta_{\text{vis},JO}$ as a function of the radius of the 2nd cation. The bold characters indicate the site that is substituted by the Pr^{3+} cascade-emitting ion. The compounds in brackets are not shown, because a determination of $\eta_{\text{vis},JO}$ was not possible due to thermal coupling.

are the Pr^{3+} -doped compounds SrYF_5 , $\text{Ba}_4\text{Y}_3\text{F}_{17}$, $\text{Ba}_{0.5}\text{La}_{0.5}\text{F}_{2.5}$, and Rb_3YF_6 , which besides a pure $5d$ emission also exhibit a thermally activated $5d$ emission at room temperature (see discussion in the previous section).

Taking into account the above-described different types of emission transitions in the Pr^{3+} -doped compounds investigated, we obtain the $\eta_{\text{vis},JO}$ values listed in Table III.

It is interesting to note that a very good approximation for $\eta_{\text{vis},JO}^{\text{high}}$ can be obtained by simply estimating $\eta_{\text{vis},JO}^{\text{high}} \approx \eta_{\text{vis},\beta} = 2 \times \beta$. In Table IV the experimentally determined branching ratios β for the $^1S_0 \rightarrow ^1I_6$ transition, $\eta_{\text{vis},\beta}$ and $\eta_{\text{vis},JO}^{\text{high}}$ are listed. This estimation holds, because almost all transitions from the 3P_0 and 3P_1 levels occur in the visible spectral range. Thus the number of photons emitted around 400 nm (the $^1S_0 \rightarrow ^1I_6$ transition) is nearly equal to the number of photons emitted in the visible range (for pure radiative decay from the 3P_0 and 3P_1 levels). Note that this equality also gives a unique method for determining the quantum efficiency of the $^3P_{0,1}$ level, because it is a self-calibrating method.^{30–32}

VII. ANALYSIS OF QUANTUM EFFICIENCY

As already stated in Sec. II, there are some known characteristics required for a material to be host material for a Pr^{3+} cascade emission. In this section we try to find the relations between the obtained values for the quantum efficiency of the cascade emission data and the characteristics of the compound, as ionic radii of the substituted and surrounding ions as well as coordination numbers. However, it will be seen, that there are no strictly valid characteristics, so the derived relations should be considered as general tendencies.

First, we look at the derived quantum efficiency, $\eta_{\text{vis},JO}$, as a function of the ionic radius of the second cation ($R_{2\text{nd}}$). In Fig. 15, we plotted $\eta_{\text{vis},JO}$ for the center exhibiting cascade emission, and these centers are indicated in bold in the figure legend. For $RE^{3+}F_3$, with $RE = \text{Y}, \text{Lu}, \text{La}, \text{Pr}$, we took $R_{2\text{nd}} = R_{RE}$. For all compounds exhibiting cascade emission, $R_{2\text{nd}}$ is smaller than 1.4 Å. None of the cascade emitters have

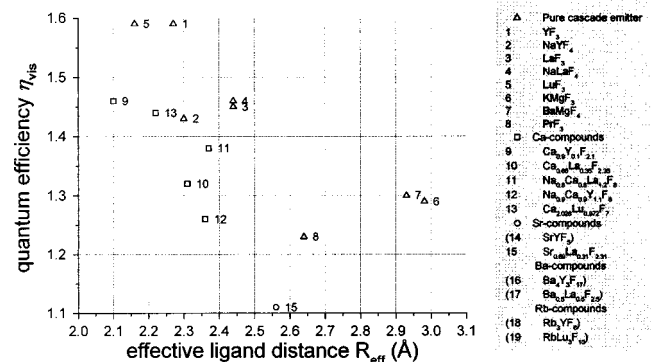


FIG. 16. Quantum efficiency $\eta_{\text{vis},JO}$ as a function of the effective ligand distance. The bold characters indicate the site that is substituted by the Pr^{3+} cascade-emitting ion. The compounds in brackets are not shown, because a determination of R_{eff} is not possible.

$R_{2\text{nd}} > 1.4$ Å. The highest quantum efficiencies (and thus also the highest values for the branching ratio β) for the $^1S_0 \rightarrow ^1I_6$ transition are obtained for $1.1 \text{ Å} < R_{2\text{nd}} < 1.3 \text{ Å}$. For smaller second cations, β drops.

Furthermore, we look at the quantum efficiencies $\eta_{\text{vis},JO}$ as a function of the effective ligand distance R_{eff} . R_{eff} is defined as $R_{\text{eff}} = R_i - 0.6 \Delta R$,³³ where R_i is the ligand distance (data from Ref. 34) and ΔR is the difference between the ionic radius of Pr^{3+} and the cation, which is substituted. R_{eff} thus takes into account the lattice relaxation. The result is plotted in Fig. 16. All the compounds investigated have $R_{\text{eff}} \geq 2.1$ Å. The highest quantum efficiencies (and thus also the highest value for the branching ratio β) for the $^1S_0 \rightarrow ^1I_6$ transition are obtained for $2.1 \text{ Å} < R_{\text{eff}} < 2.5 \text{ Å}$. For larger effective radii, $\eta_{\text{vis},JO}$ (and β) drops.

All investigated compounds with cascade emission have coordination numbers of 8 and higher for the lattice site substituted by the Pr^{3+} ion with cascade emission (see Table III).

In summary, the compounds investigated and exhibiting cascade emission are characterized by a small radius of the second cation, a large substituted lattice site, and a high coordination number. These observations therefore support the assumptions, which have already been stated in the literature.^{6,9–13} The reason is that these characteristics lead to small crystal fields on the Pr^{3+} site and finally to a small splitting of the $\text{Pr}^{3+}5d$ energy levels.

VIII. SUMMARY

We have investigated the spectroscopic properties of a variety of Pr^{3+} -doped fluoride compounds under synchrotron radiation excitation in order to find new photon cascade emitters suitable as phosphors for Xe-discharge lamps. The binary systems YF_3 , LuF_3 , and LaF_3 exhibited pure cascade emissions and showed only one emitting center. Also for NaYF_4 , NaLaF_4 , and BaMgF_4 pure cascade emissions and just one optical center were observed. In all of these compounds, there is only one suitable lattice site for the Pr^{3+} ion. The Ca compounds investigated, $\text{Ca}_{0.9}\text{Y}_{0.1}\text{F}_{2.1}$, $\text{Na}_{0.9}\text{Ca}_{0.9}\text{Y}_{1.1}\text{F}_6$, $\text{Ca}_{0.65}\text{La}_{0.35}\text{F}_{2.35}$, $\text{Na}_{0.8}\text{Ca}_{0.8}\text{La}_{1.2}\text{F}_6$, and

$\text{Ca}_{2.028}\text{Lu}_{0.972}\text{F}_7$, showed both cascade emissions and broadband $5d$ emissions occurring from two different optical centers. We tentatively assigned the cascade emission to Pr^{3+} on the rare-earth lattice site and the $5d$ emission to Pr^{3+} on the Ca^{2+} lattice site. Also for the Sr, Ba, and Rb compounds two optical centers were observed, and for $\text{Sr}_{0.69}\text{La}_{0.31}\text{F}_{2.31}$ and $\text{RbLu}_3\text{F}_{10}$ the situation is similar to that of the Ca compounds, with two optical active centers. For the other compounds, SrYF_5 , $\text{Ba}_4\text{Y}_3\text{F}_{17}$, $\text{Ba}_{0.5}\text{La}_{0.5}\text{F}_{2.5}$, and Rb_3YF_6 , thermally activated $5d$ emissions were also observed. In the Sr, Ba, and Rb compounds an assignment of an emission type to a Pr^{3+} -substituted site is not absolutely clear. We tentatively assigned the cascade emission to Pr^{3+} ions on the rare-earth site for the Sr compounds and to Pr^{3+} ions on the Ba^{2+} and Rb^+ sites for the Ba and Rb compounds. In any case, the Pr^{3+} ions also enter the compounds on lattice sites with different valences rather easily. Therefore, in general, ternary systems with suitable-sized divalent lattice sites should be avoided.

We determined the quantum efficiency for the visible spectral range with the help of the Judd-Ofelt method and from the consideration of the branching ratio of the $^1S_0 \rightarrow ^1I_6$ emission transition under consideration of the influence of other optical active centers. We found relationships

between the quantum efficiency and the ionic radii of the second cation, the effective ionic radius of the Pr^{3+} ion in the compound, and the coordination number of the Pr^{3+} ion in the compound. These observations confirmed the results obtained by our group and other groups based on a wide field of materials. The quantum efficiency includes the photons emitted at 400 nm, which cannot be directly used for phosphor lamps due to the low sensitivity of the human eye at this wavelength. Thus, the transfer partner ions for Pr^{3+} have to be found to convert the energy of this 400-nm photon into a photon at an energy more suitable for fluorescent lamps. Research in this direction is still in progress.

ACKNOWLEDGMENTS

This work was done within the frame of the BMBF project Grant No. 03N8019D as well as HASYLAB projects, Grant Nos. II-99-065 and II-01-012. The authors thank Dr. M. Kirm, M. True, and S. Vielhauer from HASYLAB for their kind supervising of the experiments and Dr. D. Schiffbauer and Dr. C. Wickleder from the Institute of Anorganic Chemistry of the University of Cologne for the structure analysis.

*Corresponding author. Electronic address: stefan.kueck@ptb.de

- ¹R. T. Wegh, H. Donker, K. D. Oskam, and A. Meijerink, *Science* **283**, 663 (1999).
- ²C. Feldmann, T. Jüstel, C. R. Ronda, and D. U. Wiechert, *J. Lumin.* **92**, 245 (2001).
- ³J. L. Sommerdijk, A. Brill, and A. W. de Jager, *J. Lumin.* **8**, 341 (1974).
- ⁴J. L. Sommerdijk, A. Brill, and A. W. de Jager, *J. Lumin.* **9**, 288 (1974).
- ⁵W. W. Piper, J. A. de Luca, and F. S. Ham, *J. Lumin.* **8**, 344 (1974).
- ⁶W. T. Carnall, P. R. Fields, and R. Sarup, *J. Chem. Phys.* **51**, 2587 (1969).
- ⁷C. G. Levey, T. J. Glynn, and W. M. Yen, *J. Lumin.* **31–32**, 245 (1984).
- ⁸I. Sokólska and S. Kück, *Chem. Phys.* **270**, 355 (2001).
- ⁹S. Kück and I. Sokólska, *Chem. Phys. Lett.* **364**, 273 (2002).
- ¹⁰S. Kück and I. Sokólska, *Appl. Phys. A: Mater. Sci. Process.* **77**, 469 (2003).
- ¹¹P. A. Rodnyi, S. B. Mikhrin, P. Dorenbos, E. van der Kolk, C. W. E. van Eijk, A. P. Vink, and A. G. Avanesov, *Opt. Commun.* **204**, 237 (2002).
- ¹²P. Dorenbos, *J. Lumin.* **91**, 91 (2000).
- ¹³P. Dorenbos, *J. Lumin.* **91**, 155 (2000).
- ¹⁴G. Zimmerer, *Nucl. Instrum. Methods Phys. Res. A* **308**, 178 (1991).
- ¹⁵S. Kück, I. Sokólska, M. Henke, and E. Osiać (unpublished).
- ¹⁶A. A. Kaminskii, in *Laser Crystals*, edited by D. L. MacAdam, Springer Series in Optical Sciences Vol. 14 (Springer-Verlag,

- Berlin, 1981).
- ¹⁷E. van der Kolk, P. Dorenbos, and C. W. E. van Eijk, *Opt. Commun.* **197**, 317 (2001).
- ¹⁸E. van der Kolk, P. Dorenbos, C. W. E. van Eijk, A. P. Vink, C. Fouassier, and F. Guillen, *J. Lumin.* **97**, 212 (2002).
- ¹⁹R. Brodmann and G. Zimmerer, *J. Phys. B* **10**, 3395 (1977).
- ²⁰E. Loh, *Phys. Rev.* **184**, 348 (1969).
- ²¹E. Loh, *Phys. Rev. B* **7**, 1846 (1972).
- ²²B. R. Judd, *Phys. Rev.* **127**, 750 (1962).
- ²³G. S. Ofelt, *J. Chem. Phys.* **37**, 511 (1962).
- ²⁴C. G. Levey, *J. Lumin.* **45**, 168 (1990).
- ²⁵R. Pappalardo, *J. Lumin.* **14**, 159 (1976).
- ²⁶B. E. Bowlby and B. di Bartolo, *J. Lumin.* **100**, 131 (2002).
- ²⁷D. S. Hamilton, P. M. Selzer, and W. M. Yen, *Phys. Rev. B* **16**, 1858 (1977).
- ²⁸W. M. Yen, C. G. Levey, S. Huang, and S. T. Lai, *J. Lumin.* **24–25**, 659 (1981).
- ²⁹L.-S. Lee, S. C. Rand, and A. L. Schawlow, *Phys. Rev. B* **29**, 6901 (1984).
- ³⁰Shi-hua Huang, Bao-jiu Chen, Xiao-jun Wang, and Mao-xun Yang, *Chin. J. Lumin.* **23**, 223 (2002).
- ³¹Shi-hua Huang, Xiao-jun Wang, Bao-jiu Chen, D. Jia, and W. M. Yen, *J. Lumin.* **102–103**, 344 (2003).
- ³²S. Kück, I. Sokólska, M. Henke, and E. Osiać, *Chem. Phys.* **310**, 139 (2005).
- ³³P. Dorenbos, *Phys. Rev. B* **62**, 15640 (2000).
- ³⁴Inorganic Crystal Structure Database (ICSD), www.fiz-informationsdienste.de